Arulkumar Muniyappan ✉
Prem Ananth Muthuvel

https://doi.org/10.21278/TOF.484059323
ISSN 1333-1124
eISSN 1849-1391

TAGUCHI OPTIMISATION OF FRICTION AND WEAR PROPERTIES OF Ti6Al4V ALLOY COATED WITH TiAlN FOR ORTHOPAEDIC APPLICATIONS

Summary

The influence of high bonding coatings of TiAlN on textured titanium alloys to enhance tribological properties is investigated using a pin-on-disc tribometer at room temperature under the following range of loads [1] (80 N, 100 N, and 120 N), sliding velocities [2] (1.25 m/s, 2.1 m/s and 3.2 m/s) and sliding distances of (1125 m, 1890 m, and 2880 m). The predicted results are obtained using the design of experiments (DOE) technique response surface methodology (RSM) [3]. The results indicate that with an increase in the applied load and sliding velocities, the specific wear rate rises. On the other hand, as the sliding velocities of various sliding distances increase, the coefficient of friction drops. Microscopic images were taken to study the surface characterisation of actual and worn surfaces. The experimental results and the predicted results of RSM show close resemblance, and hence RSM is used for the prediction of wear characteristics.

Key words: *Tribometer, Response Surface Methodology, TiAlN coating, Surface Texturing*

1. Introduction

Research in the field of biotribology aims to understand the natural functioning of biological components, and the illness developed, and to optimise medical procedures and technology, sometimes from an engineering point of view. To increase the quality of life fully and effectively, it is crucial to consider the distinctive characteristics of various biological systems. Exclusive tribological mechanisms found in natural biological components provide a fundamental background for the advancement of tribology. In the same way, improvements in tribology methodology and procedures are critical for developing bio-tribology research [4], [5]. In recent years, implants have been made of biomaterials in a combination of polymers, ceramics, and metallic materials, but there are limitations due to their inherent characteristics. Metallic implants with superior strength are made of cobalt-chromium, magnesium, titanium and stainless-steel alloys. However, these materials also produce toxic substances that can lead to disorders of the skin. Using Ti-implants will prevent the influence of load on the bone structure because of their high elastic limit. However, the issue with metallic biomaterials is the stress-shielding effect, which may lead to osteoporosis [6]. This paper discusses the effects of various surface treatments,

like grinding and electrochemical polishing, on the corrosion resistance of AISI 316L, a type of austenitic stainless steel commonly used in biomedical applications. The study found that electrochemical polishing improves pitting corrosion resistance, but mechanical defects can significantly reduce this resistance. Additionally, the paper highlights the potential dangers of nickel and other alloying elements present in steel, which can cause allergic reactions, toxicity, and even carcinogenic effects when released into the body due to corrosion [7]. In developing innovative metallic alloys with suitable properties for biomedical applications, Ti alloys have resulted in biomaterials for human fractured bone replacement. Researchers are paying great attention to improving the stress shielding effect of implants by using low Young's modulus alloys, while in turn Ti- alloy is highly recommended [8], [9].

Although Ti-alloy implants are familiar, they have several limitations. The Young's modulus of these implants is undoubtedly lower than that of stainless-steel-based, and cobalt-chromium-based alloys, but it is still higher than that of bone. Further porous implants have drawn interest because they aid in lowering Young's modulus and enhance bone ingrowth. Many titanium implants utilise alloying materials like vanadium and aluminium, which are regarded as potentially harmful. These implants have largely demonstrated their biocompatibility, but there have nevertheless been a few cases where allergies may have been brought on through the release of harmful ions into the blood. Therefore, attempts are being made to create implants that exhibit greater biocompatibility. Additionally, several surface treatments are employed to enhance the qualities of titanium alloy implants, such as bone bonding and wear and corrosion resistance [10], [11].

Currently, the problem of prosthetic hip joints is the need to increase their lifespan by improving their mechanical properties. Adding a microtextured pattern on the femoral head surfaces shows improved performance of the mechanical properties where, for example, friction and wear are reduced when compared to conventional smooth surfaced prosthetic joints [12], [13]. Surface texturing has a high impact on tribological properties, such as the friction coefficient and wear rate, altering the specimen surface roughness by creating textured patterns. Various techniques are used by researchers to create the surface texture on specimens, where laser-based surface texturing called LST has emerged as one of the most promising texturing techniques due to its superior control and accuracy [14]. To enhance the properties of materials like Ti6Al4V alloy, laser surface texturing (LST) is employed to modify the surface topography. This process creates specific patterns or features on the material surface, which can improve roughness and wettability, leading to better performance in various applications [15]. Additionally, the treatment improves the material's wear resistance and coefficient of friction [16]–[18]. Octagon-shaped circular pattern textures on biomaterials like cobalt chromium-molybdenum alloy (CoCrMo), ultra-high molecular weight polyethene (UHMWPE), stainless-steel alloy (SS) and alumina (Al_2O_3) have a lower coefficient of friction and specific wear rate than untextured specimens of these biomaterials [19]. Biocompatibility surface covering can be achieved using modern surface modification methods. Despite a bright future in biomedical applications, ceramic-coated metal composites have several drawbacks, including coating thickness, corrosion, deterioration, and debris discharges. For long-lasting, sustainable coatings, research should focus on further enhancing and managing their physiochemical properties [20].

TiN is the most popular coating due to its better biocompatibility properties. Bacterial colonisation and corrosion resistance are improved by increasing the hardness of the metallic surfaces by coating. It also causes a notable reduction in the release of metal ions into body fluids [21]. It was found that transition metal nitrides and other hard coatings are useful for surface strengthening to increase the application of Ti6Al4V alloy. Various nanostructured bioactive coatings can be created using physical vapour deposition (PVD) techniques. One of the first patented coatings for biological applications was TiN coated by PVD [22]. Texturing

has significantly increased the coating's bonding strength. Better integrity and adherence are provided by the coating's dispersion over the dimple after it has been applied to the textured surface. Better performance is also provided under shear loading circumstances by the mechanical locking of the coating [23]. By introducing chlorine atoms into the TiN coating, the prosthetic pair of SS/UHMWPE may exhibit better tribological behaviour. A specific wear rate reduction may be ascribed to the replacement of the TiN counterface with a softer TiO layer that is less aggressive on wear for the polymer surface [24], [25]. Under all the normal stresses considered, the TiAlN coating on the Ti6Al4V alloy's textured surface with a Cr interlayer demonstrated a lower wear rate. When applied to a textured surface with a chromium interlayer, the coating's bonding strength is 8% stronger than when applied to a lapped surface [26]. A study was conducted on the process of powder-mixed electrical discharge diamond grinding (PMEDDG) of Ti6Al4V. The study focused on empirical models, process investigation, the optimal setting of factors, and surface production using aluminium (Al) and silicon carbide (SiC) powder mixed with dielectric fluid. To determine the optimal process variables when using aluminium powder, the grey-based Taguchi approach was employed. The effectiveness of this method was validated by a confirmation test [27].

2. Materials and Methods

2.1 Experimental set-up

Ti6Al4V grade 5 alloys were procured in the form of rods as per ASTM G99 standards and were cut into 28 mm x10 mm dimensions using the wire cut EDM technique shown in Figure 1.a. The chemical composition and mechanical properties of Ti6Al4V are given in Tables 1 and 2.

Table 1 Ti6Al4V grade 5 alloy chemical composition [3], [28], [29]

Element	Titanium	Aluminium	Vanadium	Iron	Oxygen	Carbon
Content (%)	87.6 – 91	5.5 – 6.75	3.5 – 4.5	< 0.40	< 0.20	< 0.080

Table 2 Ti6Al4V grade 5 alloy mechanical properties [29], [30]

Property	Density	Ultimate Tensile Strength	Yield Tensile Strength	Modulus of Elasticity	Compressive yield strength	Poisson's ratio	Shear modulus
Specifications	4420 kg/m^3	1170 MPa	1100 MPa	90 GPa	970 MPa	0.342	44 GPa

Surface modification of the Ti6Al4V specimens was made using a laser surface texturing machine with an operating parameter as a laser pulse of 2 KHz, power of 10 W, wavelength of 1064 nm, scanning speed of 200 mm/s, and the loop of a single pass. Figure 3.a shows a photographic view of the laser-marking machine used for surface texturing. The octagon shape of the circular pattern textures is drawn using the AutoCAD software shown in Figure 1.b and the same can be converted into a data exchange format (DXF) for easy file exchange to other software. Laser marking machines have EZCAD software, which loads the exported DXF files from AutoCAD software. Figure 3.a shows the load AutoCAD file laser marking machine while Figure 3.b displays the laser marking operation performed for specimen-loading in the LST machine. The final top view of the specimen which is textured and coated with TiAlN is shown in Figure 1.c. According to Equation 1, there are a total of 72 dimples in the shape of octagons. The distance between the textured patterns is marked at 0.5 mm both horizontally and vertically as shown in Figure 2, while the depth of the textured patterns is set at 100 μm.

$$No.of\ dimples = \frac{[Area\ of\ pin\ specimen\ X\ dimple\ area\ density]}{Area\ of\ dimple} \quad (1)$$

A textured Ti6Al4V alloy surface is coated with titanium aluminium nitride coating (TiAlN) which is a universally accepted biocompatibility coating. The reason for this TiAlN coating lies in the addition of aluminium which leads to the formation of aluminium oxide on the surface of the material which increases the operational temperature range of the coating. The structure results in an optimal relation of high hardness to residual compressive stress, prevents any form of erosion to the inner layers of these compounds, and improves the elastic modulus [21], [22] [23].

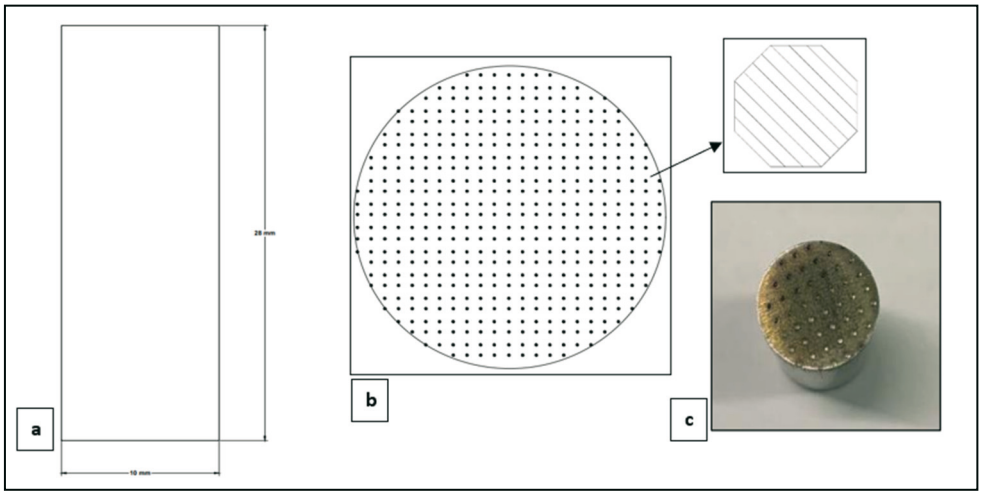

Fig. 1 a) Specimen pin with 28 mm x10 mm b) octagon texture c) textured coated Ti6Al4V alloy.

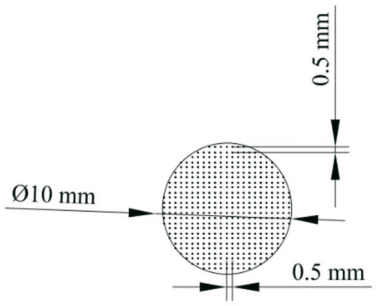

Fig. 2 Distance between the texture.

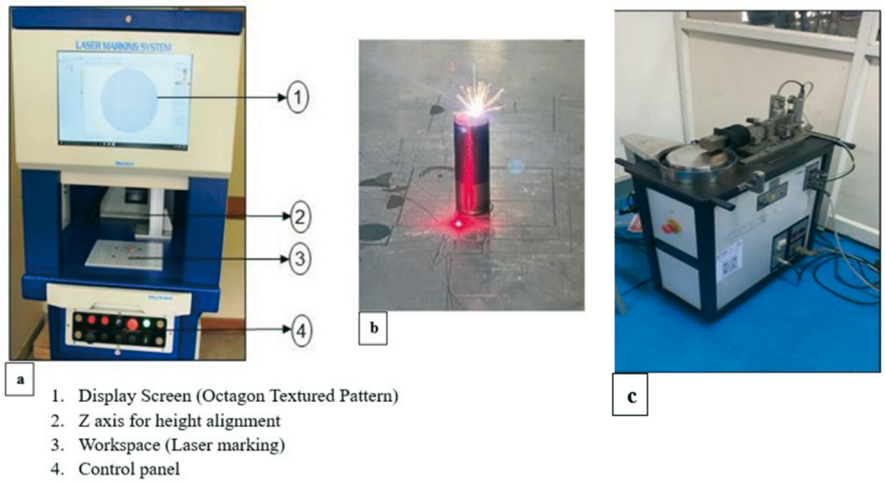

Fig. 3 a) Laser marking machine b) laser marking operation and c) pin-on-disc tribometer.

Physical vapour deposition techniques are carried out to give the TiAlN coating a thickness of 4 µm. The reason for choosing PVD coating techniques is that the coating is

provided with hard, wear, and corrosion resistance, it gives a more uniform deposit, improves adhesion and is environmentally friendly [20]. The composite coating of TiAlN deposited over the lapped surface of Ti6Al4V was observed using the high-magnification microscope Daksh Digital inverted metallurgical microscope shown in Figure 20. Using a pin-on-disc Ducom TR20 tribometer machine, dry sliding wear test experiments were carried out as shown in Figure 3.c. The following test conditions are listed in Table 3. Sliding distances of 1125 m, 1890 m and 2880 m were calculated using Equation 2 for the different sliding velocities [2] and track diameter:

$$Sliding\ distance(d) = \frac{\pi DNt}{60}\ \ in\ \text{m} \tag{2}$$

where D is the disc track diameter in mm, N is the rotating speed of the disc in rpm, and t is the testing time in mins (30 minutes per sample).

After the successful completion of each experiment, the frictional force concerning time and sliding distance was recorded using a force transducer. The recorded data were exported in the form of Excel. Equation 3 shows the calculation of the coefficient of friction using the recorded value of frictional force and the load applied value through the data acquisition system. The specific wear rate was calculated using the mass loss shown in Equation 4. Specimens were weighed before and after each test:

$$Coefficient\ of\ friction\ (\mu) = \frac{F}{N} \tag{3}$$

where F is the frictional force recorded and N is the load being applied (N)

$$Specific\ wear\ rate = \frac{v}{N\ x\ d}\ \ in\ \text{mm}^3/\text{Nm} \tag{4}$$

where v is the wear volume of the specimen after the test (mm^3) which is calculated using the mass loss in g by density of specimen (ρ) in g/cm^3, N is the load being applied (N), and d is the sliding distance (mm) which is calculated using Equation 2.

2.2 Response surface methodology (RSM)

Response surface methodology (RSM) is used to create, enhance and optimise processes using a set of statistical and mathematical techniques. By using this methodology, researchers can predict the lifetime of the machining tool and observe the surface characteristics, tribological properties and other parameters. This technique is widely employed to achieve significant improvement when two or more input parameters are affected. Design Expert software is used to create an experimental strategy for RSM. A second-order quadratic model was constructed to represent the connection between specific wear rates and the input-independent parameters. The independent input parameters such as load (A), velocity (C), distance (B) and response, such as wear rate (y), are considered for this work. The connection between the independent input and the output parameters in RSM is shown in the following equation (5):

$$y = f\ (A, B, C) \tag{5}$$

The quadratic model of y is used to identify the place where the primary target is located, based on how the output response approaches or nears its optimum value, in addition to doing research over the full factor space. By applying a face-centred central composite design in machining tests based on response surface methodology (RSM), relevant data are gathered for the quadratic models. Table 3 displays three independent input parameters and the output response at different ranges of levels.

Table 3 Independent parameters and their levels.

Parameters	Units	Low Level (-1)	Medium Level (0)	High Level (+1)
Load (A)	N	80	100	120
Sliding distance (B)	m	1125	1890	2880
Sliding velocity (C)	m/s	1.25	2.1	3.2

3. Results and discussion

The results of the machining runs were produced by the experimental design, as indicated in Table 4. For a given wear rate and friction coefficient, experimental plans were created to produce a quadratic model. The design expert programme was used to enter these results for additional investigation.

Table 4 Experimental results for specific wear rate and coefficient of friction

Run	Load (N)	Sliding distance (m)	Sliding velocity (m/s)	Specific wear rate x 10^{-3} ($mm^3/N \cdot m$)	Coefficient of friction
1	100	1125	2.1	2.66	0.3266
2	80	1125	3.2	2.50	0.2798
3	100	1890	2.1	2.79	0.3268
4	100	1890	2.1	2.79	0.3268
5	100	2880	2.1	2.84	0.3451
6	120	1125	1.25	2.90	0.3599
7	100	1890	3.2	2.82	0.3182
8	120	1890	2.1	2.94	0.3619
9	120	2880	1.25	2.98	0.3998
10	80	2880	3.2	2.61	0.2969
11	100	1890	2.1	2.79	0.3268
12	80	1890	2.1	2.52	0.2901
13	80	2880	1.25	2.55	0.3012
14	100	1890	2.1	2.79	0.3268
15	100	1890	2.1	2.79	0.3268
16	100	1890	2.1	2.79	0.3268
17	120	1125	3.2	2.95	0.3521
18	100	1890	1.25	2.74	0.3291
19	120	2880	3.2	3.01	0.3768
20	80	1125	1.25	2.45	0.2869

3.1 Pin-on-Disc experimental analysis

The Ti6Al4V alloy specific wear rate response versus sliding velocities, sliding distance and applied load is shown in Figure 4 a-c. It can be seen that the specific wear rate continuously increases with the increased sliding velocity, sliding distance and the load applied. At a load of 80 N, the closest value wear rate is achieved in the middle and higher levels of velocities such as 2.1 m/s and 3.2 m/s when compared to the lower-level velocity of 1.25 m/s. When at a load of 120 N, the wear rate trend increases with the increase of the sliding velocities. Figure 4b shows that for all applied loads, a change in behaviour of the specific wear rate is identified related to a change in the sliding velocity. Figure 4c shows that at a constant load of 80 N, 100 N and 120 N the specific wear rate rises with the increase in the sliding distance. Figure 5a-c shows the deviation in the coefficient friction versus the load, velocity, and sliding distance. The coefficient of friction shows transformation behaviour related to loads of 80 N,

100 N and 120 N. An increase in load with the trend of an increased coefficient of friction can be seen in all three sliding distances. However, the coefficient of friction values shows a decreasing trend with the rise in sliding velocity for all three loads at different sliding distances.

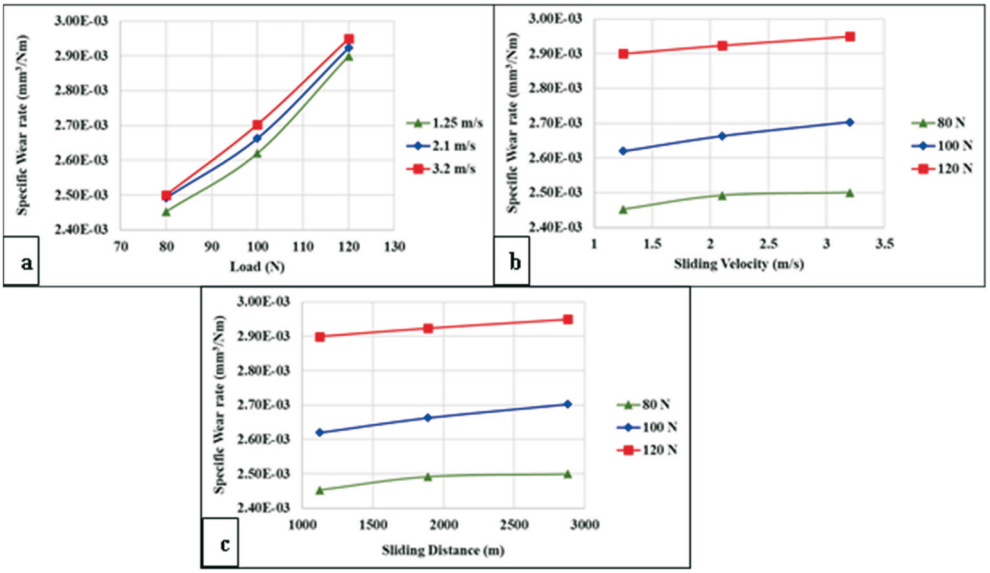

Fig. 4 Specific wear rate vs. a) load, b) sliding velocity, and c) sliding distance.

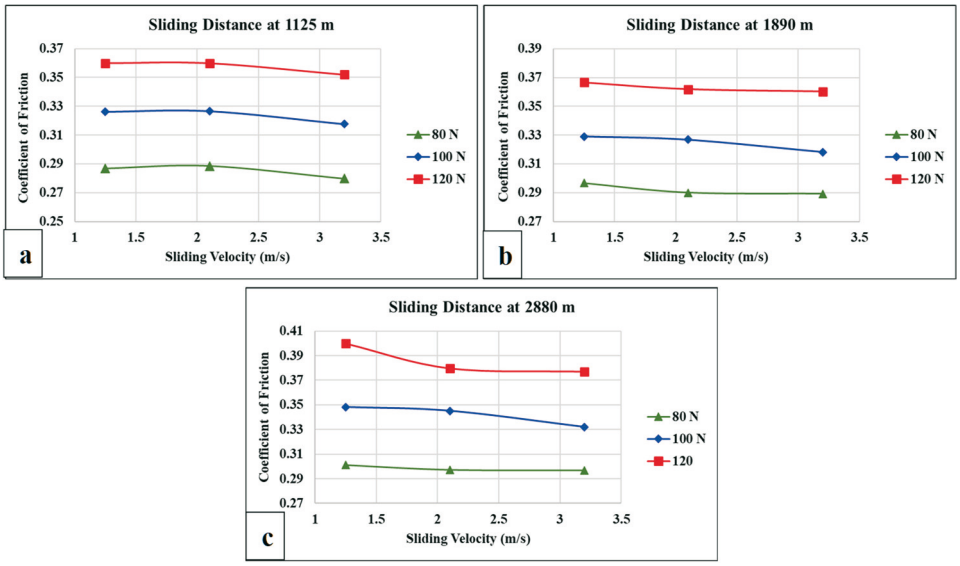

Fig. 5 Coefficient of friction vs. sliding velocity at a constant sliding distance of a) 1125 m b) 1890 m, and c) 2880 m

Deviation in the coefficient of friction versus the sliding velocity at three levels and applied loads is shown in Figure 6a-c. From Figure 6a, at a 1125 m sliding distance, both sliding velocities of 2.1 m/s and 1.25 m/s show the same trend of the plot for different applied loads, whereas the 3.2 m/s sliding velocity trends show different plots, attaining a low coefficient of friction when compared to the other two sliding velocities. From Figure 6b, at a 1890 m sliding distance, sliding velocities of 2.1 m/s and 3.2 m/s show the same value at the applied loads of 80 N and 120 N, whereas a sliding velocity of 1.25 m/s shows an increased coefficient friction at the applied loads of 80 N and 120 N. From Figure 6c, at a 2880 m sliding distance, all sliding velocities show the same value of coefficient friction at 80 N, whereas at a load of 120 N the trend shows increased behaviour for lower sliding velocities. From Figure 6a-c, it can be seen that the sliding velocities have greater influence on the coefficient of friction when compared

to the sliding distance and load. The average coefficient of friction versus the sliding distance and load is shown in Figure 7, where it can be seen that the average coefficient of friction increases with the increased load at different sliding distances. At a 1125 m sliding distance, the 80 N applied load has an average coefficient friction of 0.295, the 100 N applied load has an average coefficient friction of 0.325, and the 120 N applied load has an average coefficient friction of 0.36. However, the average coefficient friction plot shows a decreasing trend related to an increase in the sliding distance. For an applied load of 100 N, at a 1125 m sliding distance, the average coefficient friction was observed as 0.29, whereas at a 2880 m sliding distance, the average coefficient friction of 0.28 was obtained. Clearly, this shows a decrease in the value of the sliding distance. Figures 20 and 21 show the surface topography before and after conducting the pin-on-disc experimental test. These figures can be viewed using the high-magnification Daksh Digital inverted metallurgical microscope. Figure 20 exhibits the TiAlN coating over the textured surface of the Ti6Al4V alloy with magnification scales of 100 µm and 1000 µm. Figure 21 shows the wear track and fully worn-out coated textured surface of Ti6Al4V with magnification scales of 100 µm and 1000 µm.

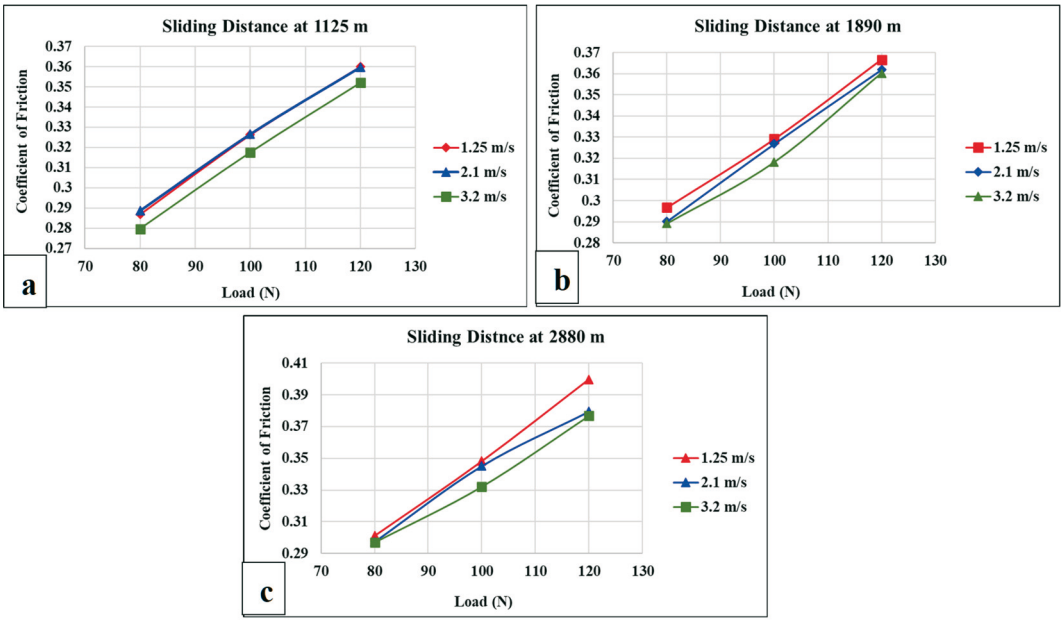

Fig. 6 Coefficient of friction vs. load at a constant sliding distance of a) 1125 m b) 1890 m and c) 2880 m

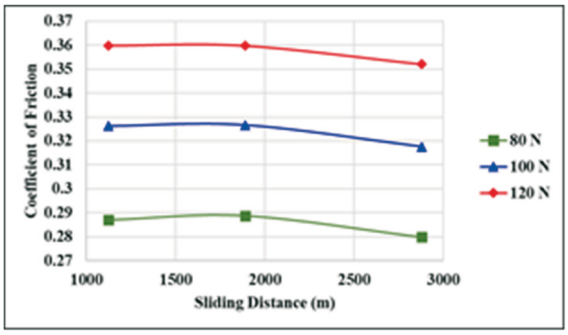

Fig. 7 Coefficient of friction vs. sliding distance at a constant load

3.2 Specific wear analysis using DOE

The importance of the model coefficient, the regression model and the lack of fit assessment is conducted in this analysis. Using the backward elimination method, the unrelated model terms are removed from the analysis table. RSM for the specific wear rate is shown in

Table 5, which indicates the importance of the "Prob. > F" model value which is less than 0.05 and suggests that the model terms have a substantial reduction in the response. Table 5 shows the "determination coefficient R^2" as a measure of the degree of fit. The best response model fits the actual data when R^2 approaches unity. It shows a lower disparity between the expected and actual values. An F model of considerable magnitude was indicated through the value of 98.81. A model F value of this magnitude has a 0.01% chance of arising due to noise. A, B, C and A^2 are considered important when compared to AB, AC, BC, B^2, and C^2 because the model "Prob. > F" is less than 0.0500. The unimportant terms are removed to improve the model terms. The "predicted R-squared" of 0.9282 agrees reasonably well with the adjusted R-squared of 0.9789. The "Adeq Precision" metric assesses the signal-to-noise ratio. A ratio greater than 4 is preferred. The Adeq Precision ratio of 34.88 in this work implies satisfactory output. This concept is useful for identifying the design space.

Equation 6 shows the final quadratic model for specific wear rates in terms of codes:

$$\text{Specific Wear Rate} = +0.0028 + 0.0002\,A + 0.0001\,B + 0.0000\,C - 7.029\text{E-}06\,AB - 2.634\text{E-}06\,AC - 2.780\text{E-}06\,BC - 0.0000\,A^2 - 0.0000\,B^2 + 7.749\text{E-}06\,C^2 \quad (6)$$

The actual factor of the specific wear rate is as follows:

$$\text{Specific Wear Rate } (mm^3/Nm) = +0.000413 + 0.000030\,\text{Load} + 2.27109\text{E-}07\,\text{Sliding Distance} + 9.96083\text{E-}06\,\text{Sliding Velocity} - 4.00509\text{E-}10\,\text{Load} * \text{Sliding Distance} - 1.35074\text{E-}07\,\text{Load} * \text{Sliding Velocity} - 3.24902\text{E-}09\,\text{Sliding Distance} * \text{Sliding Velocity} - 9.21760\text{E-}08\,\text{Load}^2 - 2.96850\text{E-}11\,\text{Sliding Distance}^2 + 8.15123\text{E-}06\,\text{Sliding Velocity}^2 \quad (7)$$

Table 5 RSM table for the specific wear rate.

Source	Sum of Squares	df	Mean Square	F-value	p-value	
Model	5.076E-07	9	5.640E-08	98.81	< 0.0001	significant
A-Load	4.614E-07	1	4.614E-07	808.37	< 0.0001	
B-Sliding Distance	2.857E-08	1	2.857E-08	50.06	< 0.0001	
C-Sliding Velocity	6.530E-09	1	6.530E-09	11.44	0.0070	
AB	3.965E-10	1	3.965E-10	0.6948	0.4240	
AC	5.568E-11	1	5.568E-11	0.0976	0.7612	
BC	6.222E-11	1	6.222E-11	0.1090	0.7481	
A^2	3.738E-09	1	3.738E-09	6.55	0.0284	
B^2	1.384E-09	1	1.384E-09	2.42	0.1505	
C^2	1.590E-10	1	1.590E-10	0.2786	0.6091	
Residual	5.707E-09	10	5.707E-10			
Lack of Fit	5.707E-09	5	1.141E-09			
Pure Error	0.0000	5	0.0000			
Cor Total	5.133E-07	19				
S.D.	0.0036		R^2		0.9889	
Mean	0.0028		Adjusted R^2		0.9789	
Coefficient of variation %	0.8650		Predicted R^2		0.9287	
			Adeq Precision		34.8088	

3.3 Friction analysis using DOE

RSM for the coefficient of friction is shown in Table 6 which indicates the importance of the "Prob. > F" model value which is less than 0.05 and suggests that the model terms have a substantial effect on the response. Table 6 shows the "determination coefficient R^2" as a

measure of the degree of fit. The best response model fits the actual data when R^2 approaches unity. It shows a lower disparity between the expected and actual values. An F model of considerable magnitude was indicated through the value of 232.15. An F model of this magnitude has a 0.01% chance of arising due to noise. A, B, C, AB, AC, and B^2 are considered important when compared to BC, A^2, and C^2 because the model "Prob. > F" is less than 0.0500. The unimportant terms are removed to improve the model terms. The "predicted R-squared" of 0.9266 agrees reasonably well with the Adjusted R-squared of 0.9909. The "Adeq Precision" metric assesses the signal-to-noise ratio. A ratio greater than 4 is preferred. The Adeq Precision ratio of 54.775 in this work implies satisfactory output. This concept is useful for identifying the design space.

Equation 6 shows the final quadratic model for the coefficient of friction in terms of code:

$$\text{Co-efficient of Friction} = + 0.3275 + 0.0396\,A + 0.0114B - 0.0053\,C + 0.0043\,AB - 0.0023\,AC - 0.0015\,BC - 0.0009\,A^2 + 0.0076\,B^2 - 0.0026\,C^2 \quad (8)$$

The actual factor of the coefficient of friction is as follows:

$$\text{Co-efficient of Friction} = + 0.134507 + 0.002195\,\text{Load} - 0.000047\,\text{Sliding Distance} + 0.022004\,\text{Sliding Velocity} + 2.42787\text{E-}07\,\text{Load} * \text{Sliding Distance} - 0.000119\,\text{Load} * \text{Sliding Velocity} - 1.71296\text{E-}06\,\text{Sliding Distance} * \text{Sliding Velocity} - 2.18265\text{E-}06\,\text{Load}^2 + 9.88938\text{E-}09\,\text{Sliding Distance}^2 - 0.002740\,\text{Sliding Velocity}^2 \quad (9)$$

Table 6 RSM table for the coefficient of friction.

Source	Sum of Squares	df	Mean Square	F-value	p-value	
Model	0.0177	9	0.0020	232.15	< 0.0001	significant
A-Load	0.0157	1	0.0157	1848.75	< 0.0001	
B-Sliding Distance	0.0013	1	0.0013	153.60	< 0.0001	
C-Sliding Velocity	0.0003	1	0.0003	33.72	0.0002	
AB	0.0001	1	0.0001	17.20	0.0020	
AC	0.0000	1	0.0000	5.07	0.0480	
BC	0.0000	1	0.0000	2.04	0.1836	
A^2	2.096E-06	1	2.096E-06	0.2474	0.6297	
B^2	0.0002	1	0.0002	18.12	0.0017	
C^2	0.0000	1	0.0000	2.12	0.1760	
Residual	0.0001	10	8.473E-06			
Lack of Fit	0.0001	5	0.0000			
Pure Error	0.0000	5	0.0000			
Cor Total	0.0178	19				
S.D.	0.0029		R^2		0.9952	
Mean	0.3293		Adjusted R^2		0.9909	
Coefficient of variation %	0.8840		Predicted R^2		0.9266	
			Adeq Precision		54.7750	

3.4 The Impact of Input Variables on the Specific Wear Rate

The suitability of the quadratic model for the specific wear rate was examined using the data provided in Table 5. The normal probability plot versus the residual shown in Figure 8 does not follow linearity but reveals the influences of the slight deviation in the input parameters, and that irregular patterns are mistakes. The predicted versus the actual value of the wear rate shown in Figure 9 follows closer to the line of equality and reveals that there is

some deviation in the influence of the input parameters which are under the permissible limit. From the above-observed limitation, derived model terms can be used to predict the specific wear rate. Within the constraints of the factors explored, the above model can be used to forecast the specific wear rate.

To investigate the impact of the input parameters, a 3D surface plot was generated as shown in Figures 10, 11 and 12. Figures 10 and 11 demonstrate that the specific wear rate rises under a normal load and falls with both a high sliding distance and a low sliding velocity. Lowering the specific wear rate is due to the formation of the thin oxide layer between the metal on metal, which acts as a sealant. Figure 12 demonstrates how the imposed normal load has an impact on the wear rate. Conversely, at a high sliding distance, the wear trends decline. This may be because of the maximum temperature rise, where the specimen surface oxidises due to the material's poor heat conductivity. This titanium alloy's oxidised surface either breaks up or becomes somewhat stable. The produced fractured oxide layer or particles can occasionally serve as lubricants, which lowers the wear rate.

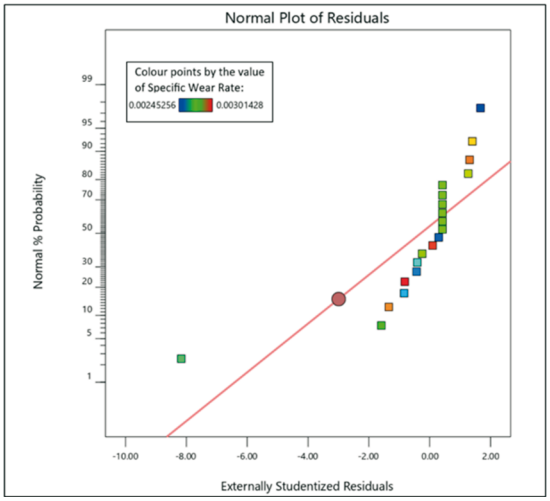

Fig. 8 Normal probability vs. residuals for the specific wear rate.

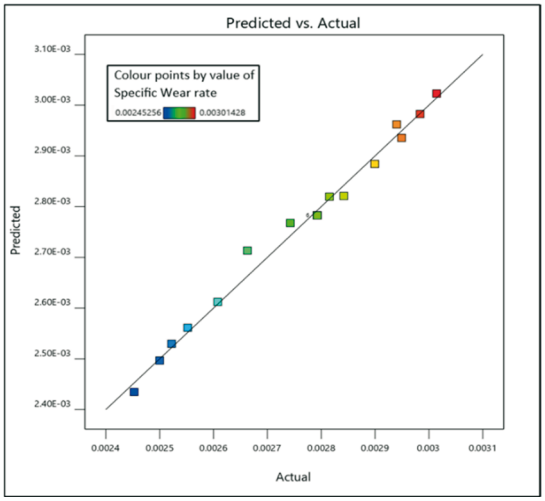

Fig. 9 Predicted vs. actual plot of the specific wear rate.

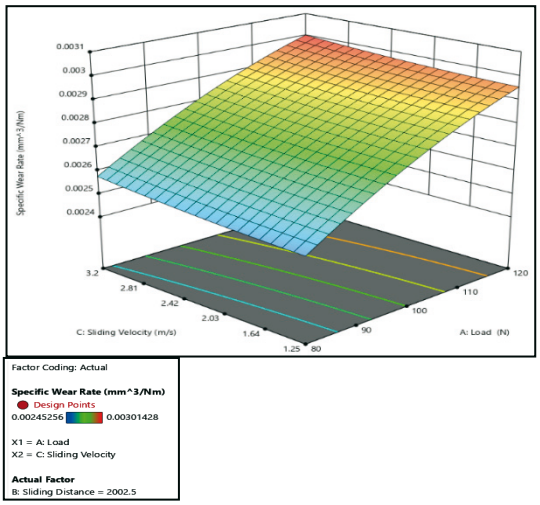

Fig. 10 Surface plot for the specific wear rate vs. applied load and sliding velocity.

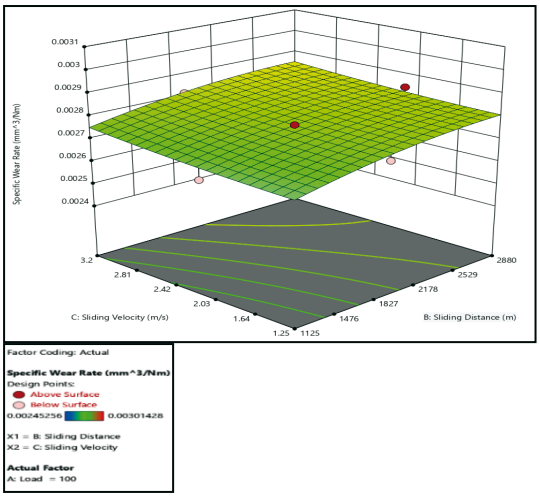

Fig. 11 Surface plot for the specific wear rate vs. sliding distance and sliding velocity.

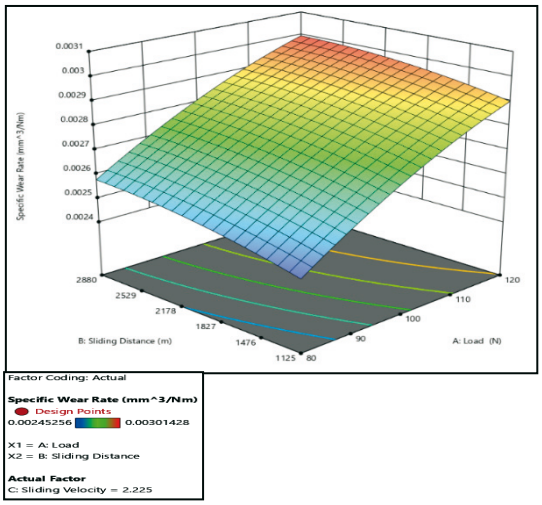

Fig. 12 Surface plot for specific wear rate vs. sliding distance and applied load.

3.5 Impact of input variables on the coefficient of friction

The suitability of the quadratic model for the friction coefficient was examined using the data provided in Table 6. Normal probability versus the residual plot is shown in Figure 13, which indicates a close association between the plots and the line of equality. However, there are some deviations from the line, which are within the permissible limits. To confirm this claim, we computed the leverage and Cook's distance and verified the results. Figure 14 shows the leverage, which reveals that the run numbers 2, 6, 9, 10, 13, 17, 19, and 20 are significant in determining the model's accuracy. On the other hand, runs 2 and 9 in the Cook's distance (as shown in Figure 15) are the subset of the leverage values and are influential values in determining the model performance. Therefore, the other values are insignificant and lie closer to the line of equality. The predicted versus the actual value of friction shown in Figure 16 follows closer to the line of equality, revealing that there is some deviation in the influence of the input parameters which is within the permissible limits. From the above-observed limitation, derived model terms can be used to predict the friction coefficient. Within the constraints of the factors explored, the above model can be used to forecast the friction coefficient.

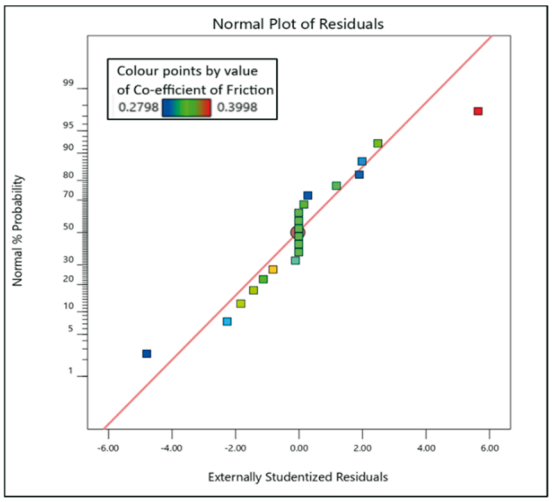

Fig. 13 Normal probability vs. residuals for the coefficient of friction.

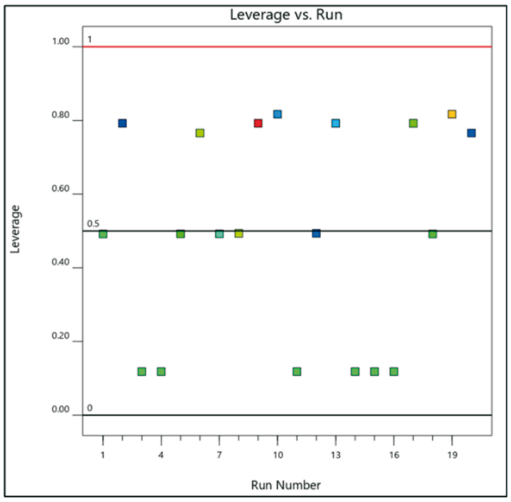

Fig. 14 Leverage vs run number.

To investigate the impact of input parameters, a 3D surface plot was generated as shown in Figures 17, 18, and 19. Figures 17 and 18 demonstrate that the coefficient of friction rises under a normal load and falls with both a high sliding distance and a high sliding velocity.

This alters the mechanical characteristics of the materials, which promotes surface deterioration and wear, reduces the contact area, and fractures the oxide layer, leading to adhesion. The test conditions determine the friction coefficient from one stage to the next, and the slide speed causes the production of a membrane protector that lessens the contact between the surfaces.

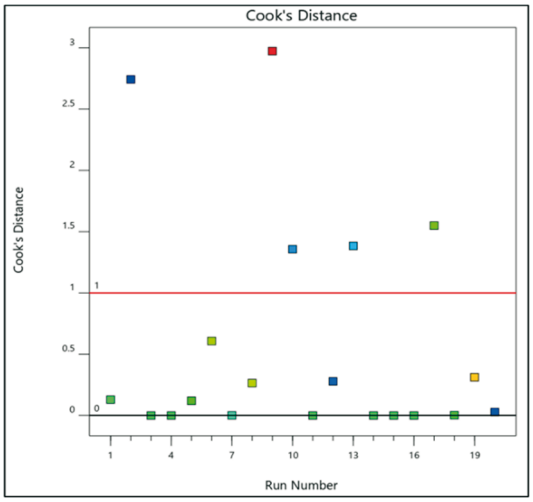

Fig. 15 Cook distance vs run number.

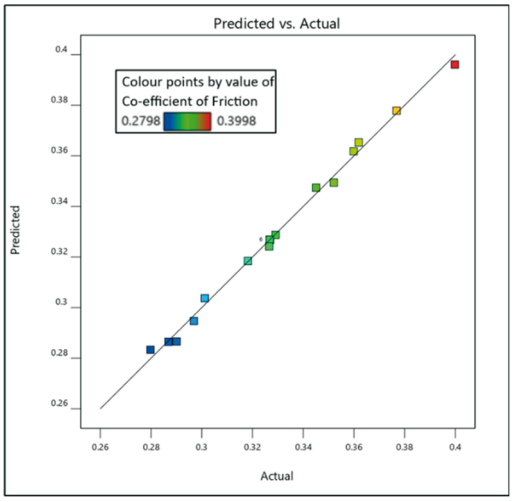

Fig. 16 Predicted vs. actual plot of coefficient of friction.

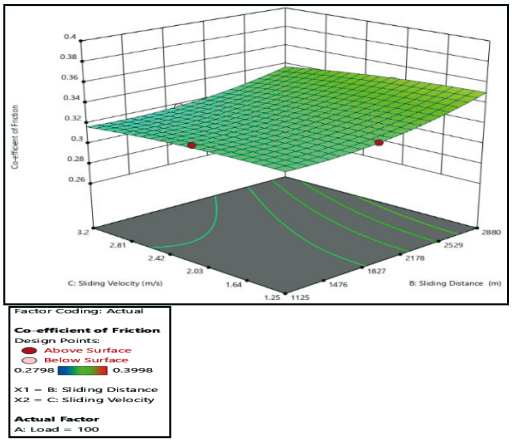

Fig. 17 Surface plot for the coefficient of friction vs. sliding distance and sliding velocity.

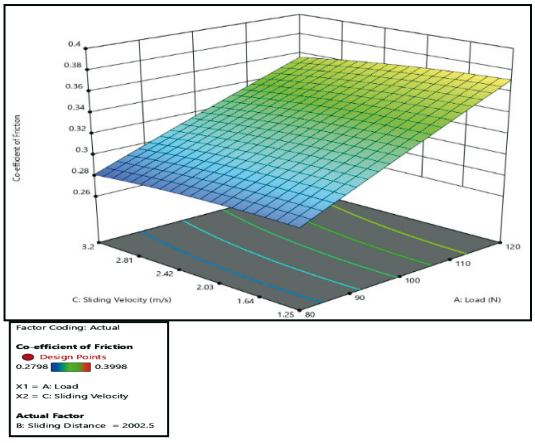

Fig. 18 Surface plot for the coefficient of friction vs. applied load and sliding velocity.

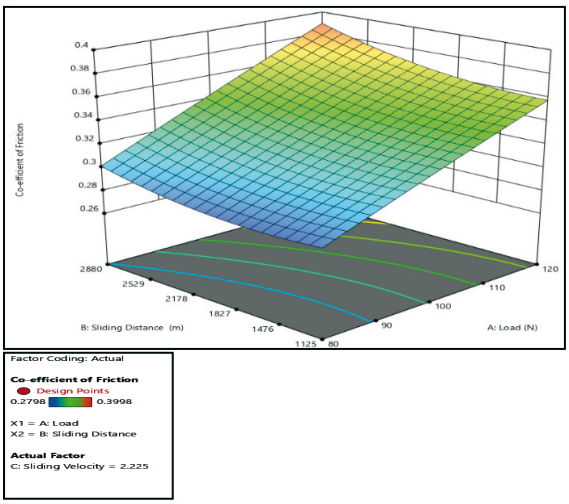

Fig. 19 Surface plot for the coefficient of friction vs. sliding distance and applied load.

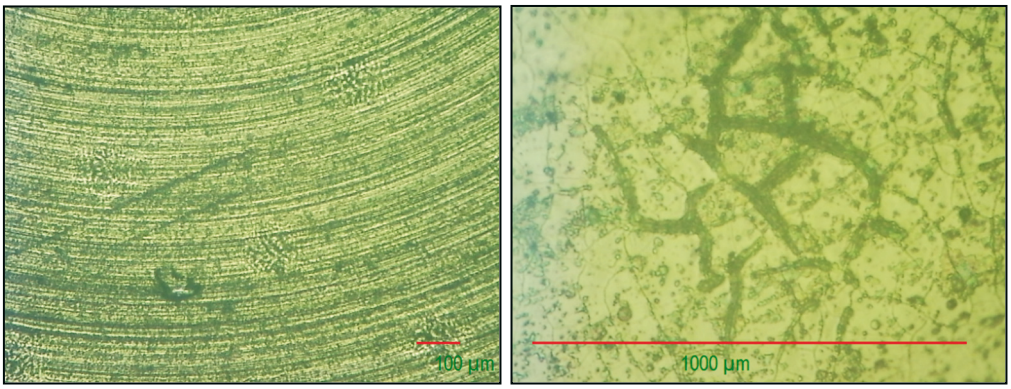

Fig. 20 Topography of the surface before the pin-on-disc tribometer test.

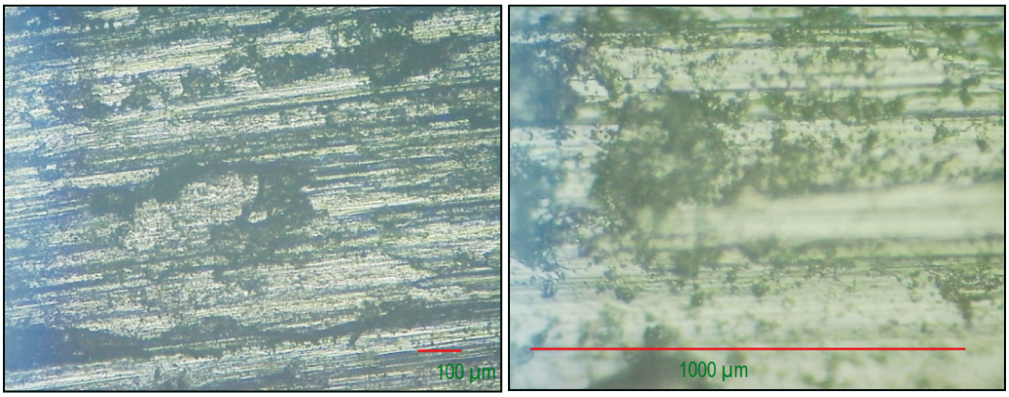

Fig. 21 Topography of the surface after the pin-on-disc tribometer test.

4. Confirmation test

The generated RSM quadratic model equations (6), (7), (8), and (9) for specific wear rates and the coefficient of friction were verified by conducting support experiments. The test run values of specific wear rates and the coefficient of friction were compared with the expected values, and it can be observed that the residual and the error percentage are minimal values as shown in Tables 7 and 8. The percentage error of the actual and predicted values of the specific wear rate is between 0.30 and 0.80, and for the coefficient of friction it is 0 and 0.2, respectively. 95% of the predicted range was observed from the result of conducting test experiments. It was concluded that the generated equations 6 to 9 from RSM are the best quadratic model equations for Ti6Al4V alloy for the given parameters.

Table 7 Comparison of experimental and predicted values for the specific wear rate.

Parameters			Specific wear rate x 10^{-3} (mm^3/N-m)			
Load (A)	Sliding distance (B)	Sliding velocity (C)	Actual	Predicted	Residual	Error %
80	1125	1.25	2.45	2.43	0.02	0.8
100	1890	2.1	2.79	2.78	0.01	0.3
120	2880	3.2	3.01	3.02	0.01	0.3

Table 8 Comparison of the experimental and predicted values for the coefficient of friction.

Parameters			Coefficient of friction			
Load (A)	Sliding distance (B)	Sliding velocity (C)	Actual	Predicted	Residual	Error %
80	1125	1.25	0.2869	0.2864	0.0005	0.1
100	1890	2.1	0.3268	0.3268	0	0
120	2880	3.2	0.3768	0.3778	0.0010	0.2

5. Conclusions

This response surface methods study was used to obtain the quadratic equations for the specific wear rate and coefficient of friction to examine the tribological behaviour of the Ti6Al4V alloy when it slides across an EN8 disc in dry conditions. Likewise, a tribometer wear test was conducted to study the effects of sliding distance, normal load, and sliding velocity over the tribological properties of Ti6Al4V alloys. Based on the results of the tribometer wear test and the RSM experimental study, the following conclusion is reached.

(i) When the normal load applied increases from 80 N to 120 N, the specific wear rate (mm^3/N-m) also increases constantly. However, for changes in the sliding velocity and sliding distance, the specific wear rate exhibits slight transitional behaviour.

(ii) The coefficient of friction increases with an increase in the applied load and decreases with an increase in the sliding distance and increasing sliding speed.

(iii) In contrast to the sliding distance and sliding velocity, the response surface approach demonstrates that the applied load has a more significant impact on the specific wear rate response. Similarly, the sliding velocity has a greater impact on the coefficient friction than the sliding distance.

(iv) The fact that the projected and experimentally observed values are reasonably close to one another suggests that the quadratic equations generated using RSM can be utilised to forecast the particular wear rate and coefficient friction of Ti6Al4V alloy with a 95% confidence level.

REFERENCES

[1] G. Bergmann et al., "Standardized loads acting in knee implants," PLoS One, vol. 9, no. 1, Jan. 2014. https://doi.org/10.1371/journal.pone.0086035

[2] R. Liu et al., "Investigation of normal knees kinematics in walking and running at different speeds using a portable motion analysis system," Sports Biomech, 2021. https://doi.org/10.1080/14763141.2020.1864015

[3] S. R. Chauhan and K. Dass, "Dry sliding wear behaviour of titanium (Grade 5) alloy by using response surface methodology," Advances in Tribology, 2013. https://doi.org/10.1155/2013/272106

[4] Z. R. Zhou and Z. M. Jin, "Biotribology: Recent progress and future perspectives," Biosurf Biotribol, vol. 1, no. 1, pp. 3-24, Mar. 2015. https://doi.org/10.1016/j.bsbt.2015.03.001

[5] W. M. Mihalko, H. Haider, S. Kurtz, M. Marcolongo, and K. Urish, "New materials for hip and knee joint replacement: What's hip and what's in kneed?" Journal of Orthopaedic Research, vol. 38, no. 7. John Wiley and Sons Inc., pp. 1436-1444, Jul. 01, 2020. https://doi.org/10.1002/jor.24750

[6] R. P. Verma, "Titanium-based biomaterial for bone implants: A mini-review," in Materials Today: Proceedings, Elsevier Ltd, 2020, pp. 3148-3151. https://doi.org/10.1016/j.matpr.2020.02.649

[7] V. Zatkalíková, M. Oravcová, P. Palček, and L. Markovičová, "The Effect of Surface Treatment on Corrosion Resistance of Austenitic Biomaterial," Transactions of FAMENA, vol. 41, no. 4, pp. 25-34, Feb. 2018. https://doi.org/10.21278/TOF.41403

[8] M. Abdel-Hady Gepreel and M. Niinomi, "Biocompatibility of Ti-alloys for long-term implantation," Journal of the Mechanical Behavior of Biomedical Materials, vol. 20. pp. 407-415, Apr. 2013. https://doi.org/10.1016/j.jmbbm.2012.11.014

[9] V. S. de Viteri and E. Fuentes, "Titanium and Titanium Alloys as Biomaterials," in Tribology - Fundamentals and Advancements, InTech, 2013. https://doi.org/10.5772/55860

[10] M. Kaur and K. Singh, "Review on titanium and titanium-based alloys as biomaterials for orthopaedic applications," Materials Science and Engineering C, vol. 102. Elsevier Ltd, pp. 844-862, Sep. 01, 2019. https://doi.org/10.1016/j.msec.2019.04.064

[11] S. Gang, F. Fengzhou, and K. Chengwei, "Tribological Performance of Bioimplants: A Comprehensive Review," Nanotechnology and Precision Engineering, vol. 1, no. 2. pp. 107-122, Jun. 01, 2018. https://doi.org/10.13494/j.npe.20180003

[12] A. Chyr, M. Qiu, J. W. Speltz, R. L. Jacobsen, A. P. Sanders, and B. Raeymaekers, "A patterned microtexture to reduce friction and increase longevity of prosthetic hip joints," Wear, vol. 315, no. 1-2, pp. 51-57, Jul. 2014. https://doi.org/10.1016/j.wear.2014.04.001

[13] H. Tekdir and A. F. Yetim, "Additive manufacturing of multiple layered materials (Ti6Al4V/316L) and improving their tribological properties with glow discharge surface modification," Vacuum, vol. 184, p. 109893, Feb. 2021. https://doi.org/10.1016/j.vacuum.2020.109893

[14] I. Etsion, "State of the art in laser surface texturing," Journal of Tribology, vol. 127, no. 1. pp. 248-253, Jan. 2005. https://doi.org/10.1115/1.1828070

[15] S. Jakovljević, D. Mezdić, G. Baršić, and H. Skenderović, "Investigation Into the Effects of Laser Texturing on the Wettability of Ti-6Al-4V Alloy," Transactions of FAMENA, vol. 45, no. 4, pp. 1-12, 2022. https://doi.org/10.21278/TOF.454031721

[16] D. Bhaduri et al., "On Design and Tribological Behaviour of Laser Textured Surfaces," in Procedia CIRP, Elsevier B.V., 2017, pp. 20-25. https://doi.org/10.1016/j.procir.2017.02.050

[17] N. Lin, D. Li, J. Zou, R. Xie, Z. Wang, and B. Tang, "Surface texture-based surface treatments on Ti6Al4V titanium alloys for tribological and biological applications: A mini-review," Materials, vol. 11, no. 4. MDPI AG, Mar. 24, 2018. https://doi.org/10.3390/ma11040487

[18] B. K. C. Ganesh, N. Ramanaiah, and P. V. C. Rao, "Effect of Surface Treatment on Tribological Behavior of Ti-6Al-4V Implant Alloy," 2012. [Online]. Available: http://www.SciRP.org/journal/jmmce. https://doi.org/10.4236/jmmce.2012.117061

[19] M. Arulkumar, R. Prashanna Rangan, M. Prem Ananth, V. Srividhyasakthi, and R. Aaditya, "Experimental verification on the influence of surface texturing on biomaterials and study of its tribological characteristics," Mater Today Proc, Jan. 2023. https://doi.org/10.1016/j.matpr.2023.01.172

[20] B. Priyadarshini, M. Rama, Chetan, and U. Vijayalakshmi, "Bioactive coating as a surface modification technique for biocompatible metallic implants: a review," Journal of Asian Ceramic Societies, vol. 7, no. 4. Taylor and Francis Ltd., pp. 397-406, Oct. 02, 2019. https://doi.org/10.1080/21870764.2019.1669861

[21] J. Narayan, W. D. Fan, R. J. Narayan, P. Tiwari, and H. H. Stadelmaier, "Diamond, diamond-like and titanium nitride biocompatible coatings for human body parts," Materials Science and Engineering: B, Volume 25, Issue 1, pp. 5-10, 1994. https://doi.org/10.1016/0921-5107(94)90193-7

[22] M. P. Nikolova, V. Nikolova, V. L. Ivanova, S. Valkov, P. Petrov, and M. D. Apostolova, "Mechanical properties and in vitro biocompatibility evaluation of TiN/TiO2coated Ti6Al4V alloy," in Materials Today: Proceedings, Elsevier Ltd, 2020, pp. 1781-1786. https://doi.org/10.1016/j.matpr.2020.05.051

[23] P. A. Muthuvel and R. Rajagopal, "Influence of surface texture on the tribological performance of AlCrN nanocomposite coated titanium alloy surfaces," Proceedings of the Institution of Mechanical Engineers, Part J: Journal of Engineering Tribology, vol. 227, no. 10, pp. 1157-1164, Oct. 2013. https://doi.org/10.1177/1350650113482826

[24] M. P. Gispert et al., "Tribological behaviour of Cl-implanted TiN coatings for biomedical applications," Wear, vol. 262, no. 11-12, pp. 1337-1345, May 2007. https://doi.org/10.1016/j.wear.2007.01.017

[25] A. Zhecheva, W. Sha, S. Malinov, and A. Long, "Enhancing the microstructure and properties of titanium alloys through nitriding and other surface engineering methods," Surf Coat Technol, vol. 200, no. 7, pp. 2192-2207, Dec. 2005. https://doi.org/10.1016/j.surfcoat.2004.07.115

[26] M. Prem Ananth and R. Ramesh, "Tribological improvement of titanium alloy surfaces through texturing and TiAlN coating," Surface Engineering, vol. 30, no. 10, pp. 758-762, Oct. 2014. https://doi.org/10.1179/1743294414Y.0000000293

[27] R. B. Sreesha, S. Chandraker, and D. Kumar, "Optimization of tribological parameters to enhance wear and friction properties of Ti6Al4V alloy using Taguchi method," Proceedings of the Institution of Mechanical Engineers, Part J: Journal of Engineering Tribology, vol. 236, no. 9, pp. 1761-1781, Sep. 2022. https://doi.org/10.1177/13506501211062540

[28] "E L E M E N T W E I G H T %." [Online]. Available: www.timet.com

[29] M. Niinomi, "Mechanical properties of biomedical titanium alloys," Materials Science and Engineering: A, Volume 243, Issues 1–2, pp. 231-236, 1998, https://doi.org/10.1016/S0921-5093(97)00806-X

[30] M. Manoj and A. Gopal, "Modelling, Investigation of Process Responses, Surface Assessment and Parametric Optimization in Powder Mixed Electrical Discharge Diamond Grinding of TI6AL4V Utilizing Grey-Based Taguchi Approach," Transactions of FAMENA, vol. 44, no. 3, pp. 93-112, Nov. 2020. https://doi.org/10.21278/TOF.44308

Submitted: 30.9.2023

Accepted: 23.4.2024

M Arulkumar*
M Prem Ananth
Department of Mechanical Engineering
Sri Venkateswara College of Engineering
Sriperumbudur – 602117, India
*Corresponding author:
arulkumar@svce.ac.in